Macromolecules

Article

Cite This: Macromolecules 2018, 51, 1041−1051

Bulk and Surface Morphologies of ABC Miktoarm Star Terpolymers Composed of PDMS, PI, and PMMA Arms

Sergey Chernyy,*[,†] Jacob Judas Kain Kirkensgaard,[‡] Jyoti P. Mahalik,[§,∥] Hyeyoung Kim,[#] Matthias M. L. Arras,[⊥] Rajeev Kumar,[§,∥] Bobby G. Sumpter,[§,∥] Gregory S. Smith,[⊥] Kell Mortensen,[‡] Thomas P. Russell,[#] and Kristoffer Almdal[†]

[†]DTU Nanotech, Technical University of Denmark, Produktionstorvet, 2800 Lyngby, Denmark

[‡]Niels Bohr Institute, University of Copenhagen, 2100 Copenhagen, Denmark

[§]Center for Nanophase Materials Sciences, [∥]Computational Sciences and Engineering Division, and [⊥]Neutron Scattering Division, Oak Ridge National Laboratory, Oak Ridge, Tennessee 37831, United States

[#]Department of Polymer Science and Engineering, University of Massachusetts Amherst, 120 Governors Drive, Amherst, Massachusetts 01003, United States

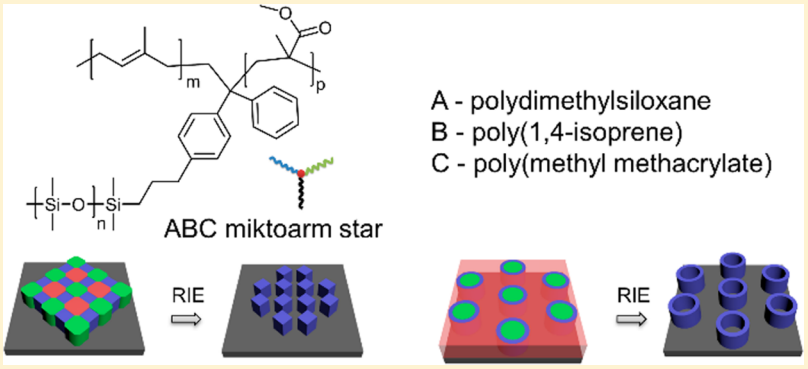

ABSTRACT: DIM miktoarm star copolymers, composed of polydimethylsiloxane [D], poly(1,4-isoprene) [I], and poly(methyl methacrylate) [M], were synthesized using a newly developed linking methodology with 4-allyl-1,1-diphenylethylene as a linking agent. The equilibrium bulk morphologies of the DIM stars were found to range from [6.6.6] tiling patterns to alternating lamellar and alternating cylindrical morphologies, as determined experimentally by small-angle X-ray scattering and transmission electron microscopy and confirmed by dissipative particle dynamics and self-consistent field theory based arguments. The thin film morphologies, which differ from those found in the bulk, were identified by scanning electron microscopy, coupled with oxygen plasma etching. Square arrays of the PDMS nanodots and empty core cylinders were formed on silica after oxygen plasma removal of the poly(1,4-isoprene) and poly(methyl methacrylate) which generated nanostructured substrates decorated with these features readily observable.

INTRODUCTION

Etch-resistant patterns formed by certain types of block copolymers, for example, block copolymers containing Si, Sn, and/or Fe atoms in one of the blocks, can be used to produce nanopatterned graphene, silicon, or polymeric substrates that have applications in semiconductor, water purification, and solar cell industries.[1−4] Lithographic potentials of linear di/triblock copolymers[5−12] have been exhaustively studied to this end, while there are relatively few reports[13−15] on the use of ABC miktoarm star terpolymers, which have a much richer diversity of morphologies and nanopatterns that can be produced.

The complexity of the architecture of the terpolymer, in comparison to linear di-, tri-, or multiblock copolymers, comes at the cost of a more detailed synthesis and purification. ABC miktoarm star terpolymers are typically produced by anionic polymerization of each arm of the star, followed by consecutively connecting the arms to a difunctional linking agent. In a typical example, lithium *p*-dimethylsilanolate functionalized 1,1-diphenylethylene was used as the initiator to polymerize a PDMS (polydimethylsiloxane) arm from the lithium silanolate, followed by the addition of a second poly(styryl)lithium arm to the free 1,1-diphenylethylenyl group and further growth of PTBMA [poly(*tert*-butyl methacrylate)] from the middle of the resultant PDMS−PS (polystyrene) diblock copolymer.[16,17] In another example, the consecutive addition of the living PI (polyisoprene), PS, and PDMS to methyltrichlorosilane produced a miktoarm star

Received: November 28, 2017
Revised: January 23, 2018
Published: February 2, 2018

DOI: 10.1021/acs.macromol.7b02485
Macromolecules 2018, 51, 1041−1051

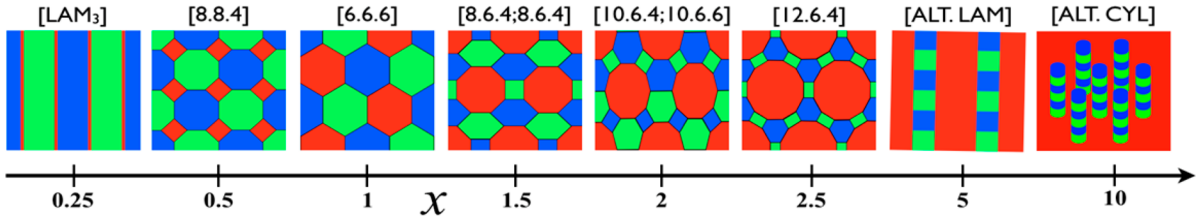

Figure 1. Generic phase diagram based on simulation predictions under the constraint of two arms (green A and blue B) having equal volumes while the third arm (red C) is varied.[20−23,44] The parameter x is the fractional length of C relative to A. The tiling patterns are labeled by a set of numbers $[k_1.k_2.k_3]$ indicating that three polygons (k_1-gon, k_2-gon, k_3-gon) meet at every vertex and repeat in a cyclic order. Tilings with more than one topologically distinct vertex are denoted $[k_1.k_2.k_3;\ k_4.k_5.k_6]$.[44]

terpolymer.[18] More recently, a trifunctional capping agent, benzaldehyde with two alkynyl units, was utilized for the synthesis of PS−PI−PFS (ferrocenylethylmethylsilane) star terpolymers.[19] In the present work we further exploit the area of Si containing ABC miktoarm stars by elaborating on DIM miktoarm stars composed of PDMS, PI, and PMMA (poly(methyl methacrylate)) arms.

Dissipative particle dynamics (DPD) and self-consistent field theory (SCFT) have been used to tackle the complexity of morphologies exhibited by ABC miktoarm stars theoretically.[20−26] Modeling of ABC terpolymers poses a challenge, due to the large number of parameters required, in comparison to diblock copolymer counterparts.[26−42] For diblock copolymers, at least two parameters are needed to simulate the morphology: volume fraction of block A, f_A, and interaction parameter, $\chi_{AB}N$, where χ_{AB} is the pairwise Flory−Huggins interaction parameter between segment A and B and N is the total number of Kuhn segments. However, for ABC terpolymers, at least five parameters are required: f_A, f_B, $\chi_{AB}N$, $\chi_{BC}N$, and $\chi_{AC}N$. Some of the modeling studies focused on benchmarking the model phase diagram results against the experimental results in which molecular weight of one of the blocks was varied, while keeping lengths of the other two arms fixed.[29,31,32] Other groups followed this by construction of the full triangular phase diagrams in which the block fractions form the sides of the triangle.[30,37,43] For simplicity, constant interaction parameters were used though the molecular weights of the blocks were changed. Two different cases of interaction parameters could be identified: Case I: all the interaction parameters are the same.[27,28,32] Case II: two of the interaction parameters are equal, and one of them is larger or smaller than the other two.[26,29]

In the idealized case I, where $\chi_{AB} = \chi_{AC} = \chi_{BC}$, a sequence of ordered patterns was predicted to form as the composition is altered under the constraint that the A and B arms are kept equal in size, while C is varied. In the balanced case, i.e., where all arms occupy equal volumes, a three-colored hexagonal honeycomb is the equilibrium morphology, as shown in Figure 1. For $0.5 < x < 2.5$ ($x = N_C/N_A = N_C/N_B$, where N_j is the number of repeats along the block j) a number of columnar structures with tiling-pattern cross section are predicted, while for larger x a hierarchical, alternating lamellar morphology [ALT.LAM] should form ($2.5 < x < 10$); for even larger x a hierarchical, alternating cylindrical morphology [ALT.CYL] is predicted. In this case, hexagonally packed cylinders with alternating layers of A and B are embedded in a matrix of C. On the basis of these simulations, we would expect a [6.6.6] morphology for $x \sim 1$; either [10.6.4; 10.6.6] or [12.6.4] or [ALT.LAM] for $x \sim 2$; [ALT.LAM] for $x \sim 5$; and [ALT.CYL] for $x \sim 10$. Experimentally, the exact location of the phase boundaries as a function of x will most likely not match Figure 1 precisely, since they are molecular weight dependent,[44] to some extent, and more importantly, the pairwise interaction parameters are not symmetric, as assumed in the simulations. Relative incompatibilities between the chains composed of PDMS−PI−PMMA arms of the miktoarm star terpolymers used in the present work could be assessed from the difference in solubility parameters (δ) of the individual homopolymers. The PMMA (δ = 18.9 $MPa^{1/2}$) and PDMS (δ = 15.1 $MPa^{1/2}$) are the most incompatible blocks, and PMMA and PI (δ = 16.4 $MPa^{1/2}$) are moderately incompatible, while PDMS and PI are the least incompatible components.[45,46] The solubility parameters were used to calculate interaction parameters for performing coarse-grained DPD simulations to probe the effect of the asymmetric interactions.

Case II,[26,43] where $\chi_{AB} \approx \chi_{AC} < \chi_{BC}$ or $\chi_{AB} \approx \chi_{AC} > \chi_{BC}$, qualitatively captures the morphologies of the poly(styrene) [S], poly(isoprene) [I], and poly(2-vinylpyridine) [V][47−50] and PS−PI−PDMS (SID)[51] miktoarm terpolymers. For the former, the interaction parameters are not balanced because $\chi_{SI} \approx \chi_{SV} < \chi_{IV}$ and for the latter $\chi_{DS} \approx \chi_{DI} > \chi_{SI}$. The SID stars having symmetric composition formed a cross-shaped morphology resembling St. Andrew's cross which we designate as the [4.8.8] tiling. This morphology is due to high incompatibility between D and the other two arms leading to the tendency of S and I domains to increase their mutual contact area to reduce the less favorable contacts with D so as to minimize the free energy of the system. Changes in the incompatibility among different monomers has been shown to have significant effect on the morphologies in the case of linear terpolymers. By keeping the composition of PI-*b*-PS-*b*-PMMA fixed and varying only the interaction parameter by partial hydrogenation of the PI block, different morphology—lamellar or network—was observed, depending on the degree of hydrogenation of PI block.[52]

In this article the bulk morphologies of DIM miktoarm star terpolymers are presented, followed by a discussion of the morphologies in thin films. Both experimental and computational results will be presented for the bulk systems, while for thin films, only experimental characterization was realized since, computationally, the number of parameters required to quantitatively describe the morphologies is prohibitive. Specifically, the lack of information about the film thickness relative to the like-domain repeat periods and the absolute as well as relative interactions of each block with the substrate and air interfaces make even qualitative comparisons between simulations and experiments unrealistic. Two of the four systems used for the bulk characterization were used for the thin film studies. The thin film morphologies were found to be different from the bulk, underscoring the importance of surface effects in defining the morphologies.

DOI: 10.1021/acs.macromol.7b02485
Macromolecules 2018, 51, 1041−1051

Scheme 1. Synthesis of the Difunctional Capping Agent, 4-Allyl-1,1-diphenylethylene (DPE-All), and ABC Miktoarm Star

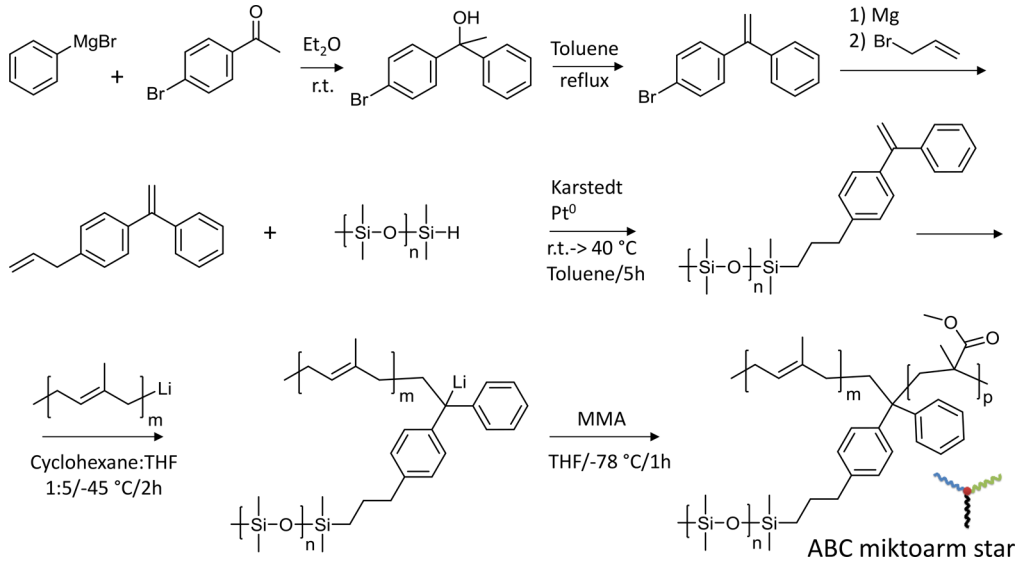

MATERIALS AND METHODS

All chemicals were purchased from Sigma-Aldrich unless otherwise stated. Tetrahydrofuran (THF) was distilled from ketyl radical of benzophenone under argon. Cyclohexane was distilled from living poly(styryl)lithium under argon. Hexamethylcyclotrisiloxane (D_3) was consecutively sublimed from calcium hydride (CaH_2) and di-*n*-butylmagnesium. Isoprene was consecutively distilled from CaH_2 and di-*n*-butylmagnesium. Methyl methacrylate (MMA) was consecutively distilled from CaH_2 and triethylaluminum (Et_3Al).

The molecular weight was determined by gel permeation chromatography (GPC) using THF with 1% triethylamine as an eluent at 0.5 mL/min flow rate with a column set consisting of a precolumn and two 300 × 8 mm main columns (PLgel Mixed C and Mixed D). For transmission electron microscopy and SAXS ~0.5 mm polymer films were produced by solvent casting from 7% THF solutions under N_2 for 1 week in the dark, followed by a thermal annealing for 5 days at 150 °C, staining with 4% OsO_4 aqueous solution for 4 h, microtoming at room temperature to 70 nm thick sections, and an additional staining with 4% OsO_4 aqueous solution on copper grids for 4 h. The TEM was performed on a FEI Tecnai T20 G^2 at 200 kV accelerating voltage in a bright field mode. The SAXS was measured using a Ganesha SAXS-LAB nm with Cu K radiation (λ = 0.154 nm). The sample-to-detector distance was 1041 mm, and the X-ray beam area was 0.04 mm^2. Thin films were spin coated from 1 to 2% toluene solutions at speeds ranging from 2 to 6 krpm and maximum acceleration (6 krpm/s) to achieve thicknesses close to the equilibrium domain spacing (d_0), followed by annealing in saturated acetone vapors for 20 h. The SEM of the microphases on silica substrates was realized on a Zeiss Supra 40VP at 1 kV accelerating voltage and 3−4 mm working distance without additional gold sputtering.

4-Bromo-1,1-diphenylethylene (DPE-Br). As shown on Scheme 1, bromobenzene (24 g, 0.228 mol) was converted to Grignard reagent by reacting it with magnesium turnings (5.7 g, 0.234 mol) in 600 mL of dry diethyl ether followed by slow addition of 4-bromoacetophenone (42 g, 0.211 mol). The reaction mixture was stirred for 0.5 h at room temperature and neutralized by 1.5 L of saturated NH_4Cl aqueous solution. After extraction with diethyl ether, the organic phase was washed with saturated NH_4Cl and water, then dried, and concentrated. Azeotropic dehydration using a Dean−Stark apparatus in toluene in the presence of catalytic amount of *p*-toluenesulfonic acid afforded a crude product which was further concentrated and distilled under reduced pressure, yielding 50 g (91%) of transparent liquid (bp 105 °C at 0.025 mbar). ^1H NMR ($CDCl_3$, 400 MHz, in ppm): 7.50 (d, J = 8.6 Hz, 2H), 7.37 (m, 5H), 7.26 (d, J = 8.5 Hz, 2H), 5.51 (dd, J = 8.1, 1.0 Hz, 2H).

4-Allyl-1,1-diphenylethylene (DPE-All). DPE-Br (30 g, 0.116 mol) was converted to Grignard reagent by reacting it with magnesium turnings (3.1 g, 0.128 mol) in dry THF, resulting in a dark brown solution to which allyl bromide (11.0 mL, 1.127 mol) was added via syringe, leading to immediate reaction as judged by the disappearance of color and the boiling of the mixture. The mixture was warmed to 65 °C for 10 min and cooled to room temperature. Standard work-up consisting of diethyl ether extraction and repetitive water washings followed by concentration on a rotary evaporator, and fractional distillation afforded 12 g (43%) of DPE-All as a transparent liquid (bp 100 °C at 0.09 mbar). ^1H NMR ($CDCl_3$, 400 MHz, in ppm): 7.39 (m, 9H), 6.06 (ddt, J = 16.8, 10.1, 6.7 Hz, 1H), 5.50 (dd, J = 9.7, 1.3 Hz, 2H), 5.16 (m, 2H), 3.48 (d, J = 6.7 Hz, 2H). Elemental analysis: theory for $C_{17}H_{16}$ 92.68% C, 7.32% H, found 92.53% C, 7.34% H. Mass spectrometry: m/z theory for $C_{17}H_{16}$ [M^+] 220.1, found 220.4. The compound (DPE-All) must be stored at −20 °C since at 4 °C slow decomposition was evidenced by a yellow discoloration.

Anionic Polymerization. The experiments were realized using an anionic polymerization setup described elsewhere.[53,54] In a typical example (Scheme 1), D_3 was polymerized using *sec*-butyllithium as an initiator in THF at −5 °C for 16 h plus 6 days at −20 °C followed by end-capping with 3 times excess of chlorodimethylsilane.[18] The PDMS-H produced was reacted with DPE-All by a hydrosilylation using Karstedt's catalyst in toluene at 40 °C, affording functionalized PDMS-DPE macromonomer. In order to link the second poly(1,4-isoprene) [PI] arm to the macromonomer, isoprene was added to the mixture of *sec*-butyllithium initiator and cyclohexane in 1L reactor and stirred for 10 h at 40 °C (*overpressure!*). Such nonpolar polymerization conditions yield poly(isoprene) characterized by 75% *cis*-1,4, 20% *trans*-1,4, and 5% 3,4 microstructure.[55,56] The solution of living poly(1,4-isoprenyl)-Li (1 equiv) was transferred to the second reactor containing excess of dried PDMS-DPE macromonomer (2 equiv) and LiCl (5 equiv) in dry THF, resulting in the development of an intense red color. After 2 h at −45 °C the reaction mixture was cooled down to −78 °C, and a predetermined amount of MMA was added. The polymerization of the MMA monomer was conducted for 1 h at −78 °C, and the resulting product was precipitated into excess of methanol.[57−59] The purification was effected by extraction of an excess of unreacted PDMS-DPE with hexane and/or fractionation in toluene/methanol mixtures. The product was dried under vacuum at 50 °C for 16 h at 0.001 mbar.

Dissipative Particle Dynamics. The simulations were performed as described previously,[60−63] except for the values of the interaction parameters between simulation beads building up the chains. The

DOI: 10.1021/acs.macromol.7b02485
Macromolecules 2018, 51, 1041−1051

coarse-graining takes a balanced $x = 1$ star as reference which is represented with three beads along each chain all attached to a central neutral junction bead. The low number is needed to be able to reach $x = 13$ which needs 39 beads along one chain. From the solubility parameters δ_i and δ_j one can calculate the χ_{ij} parameter between species i and j as

$$\chi_{ij} = v/k_BT(\delta_i - \delta_j)^2 \quad (1)$$

where k_BT is the thermal energy and v is the average volume of the two species involved as they are represented in the simulations which is dependent on the chosen coarse-graining. The calculated χ_{ij} parameters are then converted into a DPD interaction strength α_{ij} between species i and j controlling a soft potential as described in the references above:

$$\alpha_{ij} = 25 + 3.497\chi_{ij} \quad (2)$$

We get the following values for the interaction parameters: $\alpha_{DI} = 35$, $\alpha_{IM} = 55$, and $\alpha_{DM} = 91$. We will discuss the validity of these values based on this simple solubility parameter approach below when comparing simulation results with the experimental structure determination.

Self-Consistent Field Theory (SCFT). The SCFT of ABC miktoarm star terpolymer melts has been described previously.[23,24,26,29,64,65] Briefly, the Hamiltonian of the ABC miktoarm melt was defined, followed by standard field theoretical transformations leading to a field theoretical representation. The standard saddle-point approximation leads to a set of nonlinear SCFT equations, which were then solved iteratively to obtain the spatial distribution of the volume fraction of the polymer segments. The modified diffusion equations appearing at the saddle point were solved using the pseudospectral method.[66,67] Polyswift ++ provides an efficient implementation of the SCFT of ABC miktoarm star terpolymer melts and was used for all the SCFT calculations in this work.[68] Other details for evolving the SCFT equations are presented in ref 67. The Hamiltonian of the ABC miktoarm polymer is briefly described here, and finer details are described in refs 26 and 29. Three Gaussian chains, each of length N_il_i, are defined, where i is the index of the block ($i = 1$, 2, 3 represents D, I, and M, respectively); N_i and l_i stand for the number and length of a Kuhn segment in ith block, respectively. The polymer segments interact with dissimilar polymer segments by an effective short-range mean-field term defined as χ_{ij} where i varies between 1 and 2 and j varies between 2 and 3 ($j > i$). All the l_i's are assumed to be the same ($l = 0.51$ nm), where $l = v^{1/3}$ and v is the geometric mean of the molar volume of all three monomers. N_i of each polymer is obtained by equating the coarse-grain model contour length against atomistic contour length.

$$N_i = (2DP - 1)b/l \quad (3)$$

where DP is the degree of polymerization, defined as polymer molecular weight/monomer molecular weight, b is the atomistic backbone bond length (b = C−C bond length = 0.154 nm for PI and PMMA and b = Si−O bond length = 0.163 nm for PDMS). All the length scales are scaled with respect to $R_g = l(N/6)^{1/2}$, where $N = \sum_{i=1}^{3}N_i$. For all calculations, the chain fraction $f_i = N_i/N$ is assumed to be equal to the volume fraction and N is used to estimate the interaction parameter, $\chi_{ij}N$. ABC miktoarm polymer melts are reported to change morphologies over a narrow range of volume fractions, especially around symmetric composition, which justifies the choice of volume fraction for modeling the system.[29,31] The pairwise interaction parameters were obtained from the studies reported in the literature: χ_{DM} is reported to be ∼0.19 at 150 °C, the annealing temperature used in our work,[12] χ_{IM} is reported to be ∼0.08 at 50 °C[69] (assumed to be the same at 150 °C here), and χ_{ID} is reported to be ∼0.08 based on solubility parameter estimation[70] but was found to better fit our observations if a value of 0.0754 was used. Zone annealing was used to equilibrate the system.[42,71] The length and interaction parameters are given in Table 1. Simulation box parameters for the SCFT calculations are as follows: Δ is the uniform grid size, and $N_xN_yN_z$ are the number of grids in the x, y, and z directions, respectively. For DIM-0.8, DIM-2.0, and DIM-4.9, calculations were performed in two dimensions (2D) whereas three-dimensional (3D) calculation was performed for DIM-13. For the 2D calculations, $\Delta = 0.15R_g$, $N_x = N_y = 64$, and $N_z = 1$ and for the 3D calculations; $\Delta = 0.30R_g$ and $N_x = N_y = N_z = 32$ were used.

Table 1. Length and Interaction Parameters of the DIM Miktoarm Melt, Where f_i Is the Chain Fraction of Component i and $N = \sum_{i=1}^{3}N_i$

	f_D	f_I	f_M	N	$\chi_{ID}N$	$\chi_{IM}N$	$\chi_{DM}N$
DIM-0.8	0.36	0.38	0.26	368	27.7	29.4	69.9
DIM-2.0	0.25	0.26	0.49	520	39.2	41.6	98.8
DIM-4.9	0.14	0.15	0.71	878	66.2	70.2	166.7
DIM-13	0.07	0.07	0.86	1819	137.2	145.5	345.5

Static Structure Factor from SCFT. A discrete Fourier transform was used to obtain the static structure factor from the volumetric mean of the electron scattering length density (SLD), $\rho(x,y,z)$, to qualitatively model the SAXS experiments, where $\rho(x,y,z) = \sum_{i=1}^{3}SLD_i\phi_i(x,y,z)$ and SLD_i and ϕ_i represent the SLD and volume fraction of the component i at equilibrium, respectively ($z = 0$ for 2D calculations). The SLD (in 10^6 Å^{-2}) for D, I, and M components are 8.8, 8.6, and 10.8, respectively.[58] The FFTW library[72] was used to perform Fourier transformation of $\rho(x,y,z)$: $\Omega(q_x,q_y,q_z) = FT\{\rho(x,y,z)\}$, where $q_x = 2\pi l/L_x$, $q_y = 2\pi m/L_y$, and $q_z = 2\pi n/L_z$ are the scattering wave vector components in the x, y, z. L_x ($=N_x\Delta$), L_y ($=N_y\Delta$), and L_z ($=N_z\Delta$) are the length of the simulation box in the x, y, and z directions, respectively, and l, m, and n are integers ranging from 0 to $N_x/2$, $N_y/2$, and $N_z/2$, respectively. The static structure factor $S(q^*)$ is obtained as a function of $q^* = (q_x^2 + q_y^2 + q_z^2)^{1/2}$ using $S(q^*) = \langle\Omega(\mathbf{q}^*)\Omega(-\mathbf{q}^*)\rangle/(N_xN_yN_z)$ where $\Omega(\mathbf{q}^*)$ and $\Omega(-\mathbf{q}^*)$ represent the Fourier transform of $\rho(x,y,z)$ and its complex conjugate, respectively ($\mathbf{q}^*$ is a dimensionless vector). The angular brackets $\langle\ \rangle$ represent the averaging over the Fourier space.

RESULTS AND DISCUSSION

Synthesis. The synthesis of PDMS containing miktoarm stars was realized by developing a new protocol relying on a novel double functional capping agent, 4-allyl-1,1-diphenylethylene (DPE-All). The capping agent was successfully synthesized and immobilized onto hydride terminated PDMS through a hydrosilylation reaction facilitated by Karstedt's catalyst. In general, the hydrosilylation reaction is sensitive to the substitution of an alkene: terminal monosubstituted alkenes were found to be the most reactive, while internal and 1,1-*gem* double bonds are less prone to react.[73,74] Even selective hydrosilylation of monosubstituted alkenes in the presence of internal alkenes was reported.[75] Capitalizing on the high regioselectivity of the hydrosilylation process we reacted the allyl group of DPE-All with PDMS-H while retaining 1,1-diphenylethylene functionality. The progress of the reaction could be conveniently monitored by the disappearance of a heptet at 4.70 ppm (RMe_2Si-H) and appearance of a doublet of doublets at 5.42 ppm originating from the olefinic DPE protons in the modified PDMS. The PDMS-DPE macromonomer produced was further reacted with living poly(isoprenyl)-Li at −45 °C. Attempts to conduct the reaction at lower temperatures were not successful, due to the reduced reactivity of poly(isoprenyl)-Li. In the final step, a 5× molar excess of LiCl relative to the initiator was used to reduce the nucleophilicity of the growing PMMA-Li centers, which would otherwise be active enough toward the carbonyl groups of the monomer/polymer. As a result, well-defined miktoarm star block terpolymers were obtained (Table 2 and Figure 2).

DOI: 10.1021/acs.macromol.7b02485
Macromolecules 2018, 51, 1041−1051

Table 2. Characteristics of the Synthesized Star Block Terpolymers

name[a]	MW, kDa (NMR)	PDI (GPC)	Dx Iy Mz volume ratios x:y:z (NMR)[a]	morphology (SAXS)[b]	d_0[b] (SAXS), nm
D	16.1	1.07	1:0:0	n/a	n/a
I	16.4	1.03	0:1.1:0	n/a	n/a
DI	32.5	1.05	1:1.1:0	n/a	n/a
DIM-0.8	46.5	1.08	1:1.1:0.8	HEX	28.9
DIM-2.0	71.7	1.06	1:1.1:2.0	LAM	40.8
DIM-4.9	131	1.14	1:1.1:4.9	LAM	54.6
DIM-13	287	1.07	1:1.1:13.0	HEX	56.0

[a]Volume ratios (v:v:v) of the blocks were estimated by ^{1}H NMR ($CDCl_3$, 400 MHz) using densities of PDMS (0.965 g/mL), poly(1,4-isoprene) (0.91 g/mL), PMMA (1.18 g/mL) and the following NMR peaks (in ppm): PDMS ($-CH_3$) 0.07, PMMA ($-O-CH_3$) 3.60, and PI (olefinic H) 4.68, 4.76, 5.12. [b]Hexagonally packed cylinders (HEX) and lamellar (LAM) morphologies were determined from SAXS relative peak positions. The equilibrium domain spacing ($d_0 = 2\pi/q^*$) was calculated from SAXS.

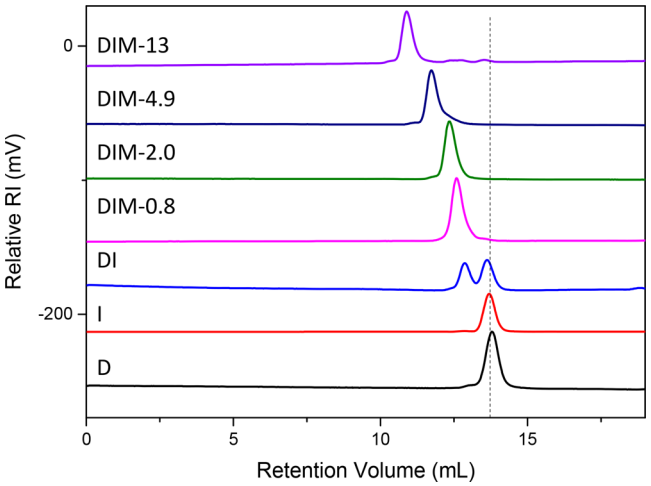

Figure 2. GPC curves of the synthesized DIM stars and their precursors.

TEM. The analysis of the bulk morphologies by TEM (Figure 3) indicate that sample DIM-0.8 forms well-ordered [6.6.6] tiling patterns in agreement with the volume fractions of the corresponding DIM arms (1:1.1:0.8, v:v:v). Since all samples were exposed to OsO_4 vapor, the PI component was selectively stained and appears black, while PMMA and PDMS, even though unstained, still have sufficient natural contrast and appear gray and white, respectively. A slightly higher PI content relative to PDMS and PMMA in DIM-0.8 results in visually larger black domains in the cross section compared to gray and white domains (Figure 3A). A similar [6.6.6] symmetry was observed for ISV stars composed of polyisoprene (I), polystyrene (S), and poly(2-vinylpyridine) (V) having almost identical volume ratios (1:1.1:0.7, v:v:v) but a 3 times higher total molecular weight (46.5 vs 134 kDa).[47,49] The morphology of DIM-2.0 and DIM-4.9 is represented by alternating lamellar [ALT.LAM] structure, which consists of PMMA lamellae separated by combination of PI and PDMS lamellae. Since PI and PDMS domains resemble cylinders, the structure is sometimes referred to as lamellar + cylinder.[20] Such a morphology was observed for ISV (1:1:3, v:v:v) and PS−PI−PFS (1:1.4:4.7, v:v:v) miktoarm star terpolymers and was predicted theoretically for ideal ABC star terpolymers over a broad composition range ($1{:}1{:}x$, $2.5 \leq x \leq 6.5$).[19,22,76] The equilibrium bulk morphology of DIM-13 is best described by the cylinders made up of stacked disks of alternating PI and PDMS in a matrix of PMMA. This morphology is referred to as a columnar piled disk[20] or lamellar-within-cylindrical structure[77] in the literature and designated as alternating cylinders [ALT.CYL] in the present work.

SAXS. The morphologies of DIM miktoarm star terpolymers in the bulk were also investigated using SAXS after thermal annealing (Figure 4). The calculated electron densities (10^{23} electrons/cm^3)[78] for PDMS (3.13), PI (3.06), and PMMA (3.83) indicate that the contrast between PDMS and PI components is low, and these microdomains will be difficult to distinguish by SAXS. Therefore, the main contribution to scattering profiles in Figure 4 arises from the size and shape of the PMMA microdomains and the spatial correlations of this microdomain. For DIM-0.8, the six reflections at scattering vector (q) ratios of $1{:}\sqrt{3}{:}\sqrt{4}{:}\sqrt{7}{:}\sqrt{13}{:}\sqrt{16}$ relative to the first-order peak (q^*) were observed, characterized by a $d_0 = 2\pi/q^* = 28.9$ nm ($q^* = 0.217$ nm^{-1}), indicating that the PMMA arrange in hexagonally packed cylindrical [HEX] microdomains with a unit cell size $a = 2d_0/\sqrt{3} = 33.4$ nm. This is consistent with the [6.6.6] tiling seen in the TEM images and with our DPD modeling as well as SCFT SAXS predictions.[26]

With an increase in PMMA molecular weight, the scattering profile indicates that the PMMA microdomains are lamellar [LAM], in keeping with the TEM and DPD results. For DIM-2.0, the lamellae have a d_0 of 40.8 nm ($q^* = 0.154$ nm^{-1}). For DIM-4.9 the d_0 of the [LAM] microdomains increases to 54.6 nm. Again, in keeping with the DPD predictions and the TEM results, the [LAM] transforms into [HEX] cylindrical microdomains for the largest molar mass of PMMA, DIM-13, although the peaks are less pronounced than for the low molecular weight sample. The two low q peaks can be indexed as the $1{:}\sqrt{3}$ peaks of the hexagonal peak sequence leading to a $d_0 = 56.0$ nm ($q^* = 0.112$ nm^{-1}), giving a unit cell size of 64.7 nm. From these results, it follows that the morphology of the DIM miktoarm terpolymers changes from [HEX] to [LAM] and then back to a [HEX] structure due to an increase in the PMMA molecular weight which causes a progressively higher degree of compositional asymmetry. These results are in agreement with the modeling data depicted in Figure 1, despite the inherent simplifications in the simulations.

SCFT Modeling. Morphologies of the DIM miktoarm polymer melts simulated using the SCFT are shown in Figure 5. Overall, the morphologies agree with the experimental micrographs shown in Figure 3 with the only exception being the case of DIM-13 where core-shell cylinders, instead of stacked alternative cylinders of PI and PDMS, are predicted. As per the parameters listed in Table 1, the repulsion between PDMS and PMMA is far stronger in comparison to other pairs, which results in the preference, in the simulations, for an inner cylindrical microdomain of PDMS surrounded by PI which shields it from nonfavorable interactions with PMMA (i.e., a core−shell morphology). One possible origin for this discrepancy is that the interactions between the PDMS and PMMA are mediated by the presence of the solvent during the preparation of the TEM samples, decreasing the nonfavorable interactions between these segments. Evidence for this is seen in the DPD simulations where the [ALT.CYL] morphology for DIM-13 was observed using symmetrical interaction parameters only. When the interaction parameters were estimated from

DOI: 10.1021/acs.macromol.7b02485
Macromolecules 2018, 51, 1041−1051

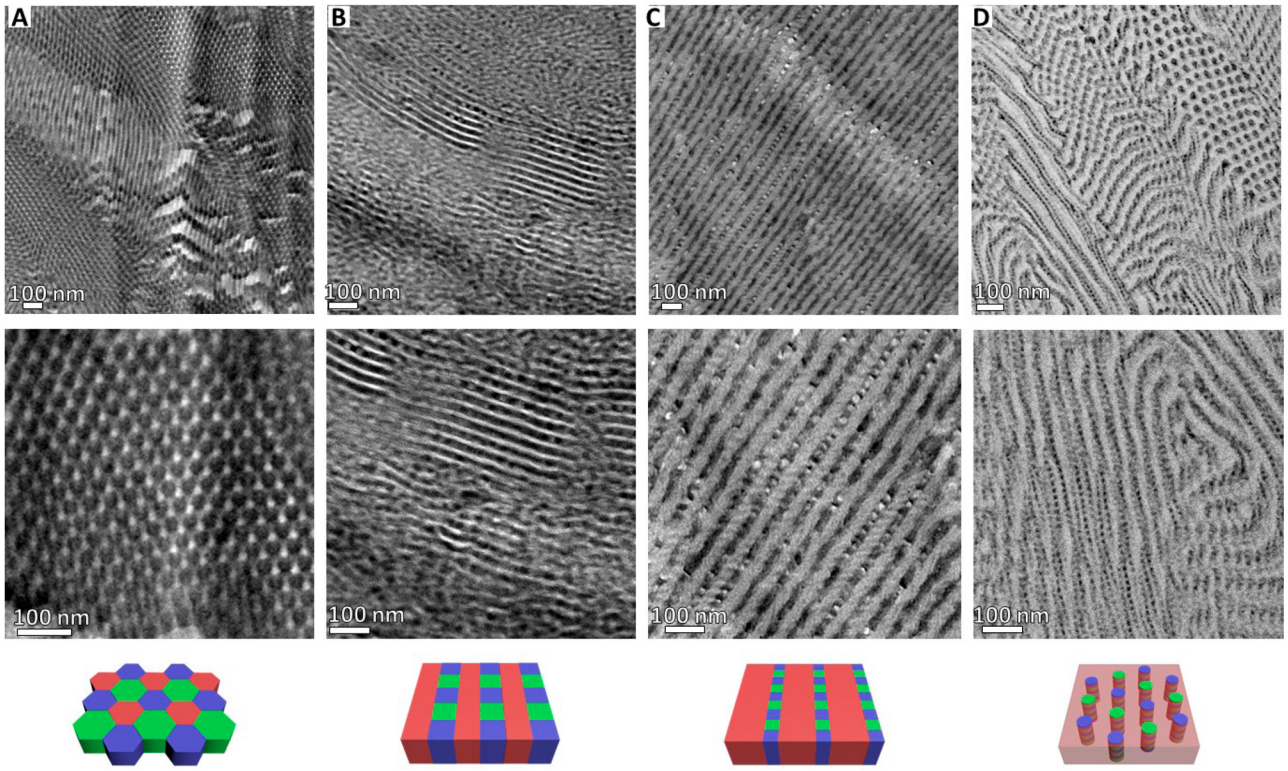

Figure 3. Top two rows: TEM images of OsO_4-stained DIM-0.8 (A), DIM-2.0 (B), DIM-4.9 (C), and DIM-13 (D) with (bottom row) the corresponding computer generated 3D bulk morphologies. Color code: D = blue, I = green, and M = red.

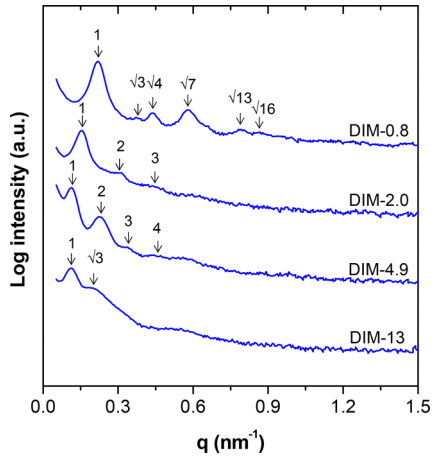

Figure 4. SAXS intensity profiles as a function of scattering vector (q) for DIM miktoarm terpolymers. The samples were prepared using solvent casting and thermally annealed at 150 °C under vacuum for 5 days. The intensity profiles were vertically shifted according to the molecular weight of PMMA. The black arrows are q/q^* values while the red arrows show DI correlation peak.

solubility parameters, the DPD simulations returned a core−shell morphology for DIM-13, in agreement with SCFT predictions. The [6.6.6] tiling and alternate lamellar structures for DIM-0.8 and DIM-4.9, respectively, prevail over other structures. However, there seems to be an ambiguity between [12.6.4] tiling structure and alternate lamellar structure for DIM-2.0. Even though DIM-2.0 and DIM-4.9 appear alternate lamellar, they are closer to a knitting pattern.

The static structure factors obtained for different compositions of DIM are shown in Figure 6. The DIM-0.8 shows relative peaks at $1:\sqrt{3}:\sqrt{4}:\sqrt{7}$, which qualitatively agrees with the peaks observed in the experimental SAXS data (Figure 4) and with the SCFT predictions by others.[26] The first peak is split into two subpeaks in Figure 6a, which is attributed to the imperfect match between the computational lattice parameters and the period of the ordered phases.[26] The DIM-2.0 and DIM-4.9 exhibit peaks at 1:2:3 positions corresponding to the lamellar spacing of PMMA as well as smaller peak designated as 1* in Figure 6b,c. Since the electron contrast between PMMA and the other two components is much higher compared to the contrast between PDMS and PI, relatively small peak is expected for the lamella formed by PDMS and PI domains. The peaks spaced as 1:2:3 are observed experimentally by SAXS for DIM-2.0 and DIM-4.9 (Figure 4), but the predicted 1* peak was not detected. This is attributed to the low intensity of the 1* peak which makes it difficult to resolve such a feature experimentally. Finally, for DIM-13, the modeled peaks, $1:\sqrt{3}:\sqrt{4}:\sqrt{9}:\sqrt{13}$, agree with $1:\sqrt{3}$ experimental ones.

We should point out that the results presented in Figure 5 and, in turn, Figure 6 were obtained by solving the SCFT equations after starting from the field configurations initialized with random numbers and by ramping up the Flory chi parameters gradually to the values presented in Table 1. We have compared free energies of the morphologies obtained with initial configurations generated by different seeds for the random number generator and, in some cases, with the inclusion of conformational asymmetry between the blocks in an *ad hoc* manner. These comparisons of the free energies have revealed that the sample DIM-2.0 can have multiple metastable structures with their free energies quite close to each other, in agreement with previous reports in the literature.[44] All of the other samples exhibited clear free energy minima. The pseudospectral method used to solve the SCFT equations is

DOI: 10.1021/acs.macromol.7b02485
Macromolecules 2018, 51, 1041−1051

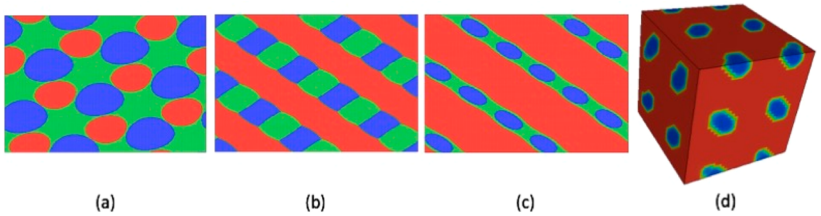

Figure 5. Evolution of bulk morphology of DIM-*x*, where *x* is varied between 0.8 and 13 and other parameters used in the SCFT calculations are presented in Table 1. (a) DIM-0.8: Archimedean tiling [6.6.6]; (b) DIM-2.0: alternating lamellar; (c) DIM-4.9: alternating lamellar; (d) DIM-13: core-shell cylinder. Color code: D = blue, I = green, and M = red. SCFT calculations yield volume fraction distribution of the respective components in the simulation box. The highest volume fraction at every grid is used to color code the morphology in this figure.

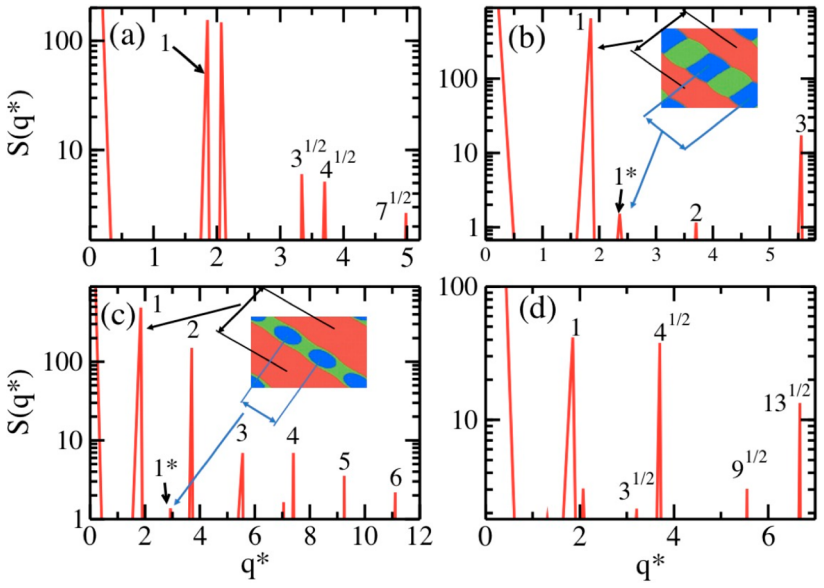

Figure 6. Static structure factor of different morphologies: (a) DIM-0.8, (b) DIM-2.0, (c) DIM-4.9, and (d) DIM-13. The peaks correspond to hexagonally packed structure for DIM-0.8 and DIM-13, whereas for DIM-2.0 and DIM-4.9 the peaks correspond to lamellar structure. The peak 1* corresponding to a smaller length scale (DI lamellar) is also observed for DIM-2.0 and DIM-4.9, and the insets in (b) and (c) show the corresponding length scales. The model structure factor results qualitatively agree with the experimental SAXS data.

quite useful for exploring different morphologies without any *a priori* knowledge of their symmetry but cannot be used to resolve infinitesimal differences in the free energies in a reliable manner. Figure 5 reveals that indeed a minimal model constructed here while ignoring the effects of conformational asymmetries and for fixed values of the Flory's chi parameters taken from the literature can reproduce the experimental results. We plan to present many details of the SCFT based modeling of ABC star terpolymers along with the effects of the conformational asymmetries in a forthcoming publication.

Thin Film Morphologies. In the thin film regime the morphologies are influenced by the interactions between the blocks and the two interfaces: substrate (silica) and free surface (air). The arms with low surface tension—PDMS (γ_{PDMS} = 21 mN/m) and PI (γ_{PI} = 31 mN/m)—would tend to preferentially segregate to the polymer/air interface, while PMMA (γ_{PMMA} = 41 mN/m), the most polar of the blocks, would preferentially segregate to the substrate (the thin silicon oxide layer coating the silicon substrate).[46] As a consequence, the equilibrium morphology for DIM-2.0 transforms from [ALT.LAM] in the bulk to a [4.8.8] tiling pattern in thin films (compare Figures 3B and 7A). Since the thickness of the films (40 nm) was close to the equilibrium domain spacing (d_0 = 40.8 nm) and the wetting is antisymmetric, a monolayer of DIM stars was achieved with all components present at the air interface, resulting in a relatively nonfrustrated morphology oriented orthogonal to the film surface.[79]

Another important effect originates from the confined movement of the ABC junction points which are allowed to migrate only in one dimension compared to the two-dimensional movement of connecting points in AB block copolymers.[49,80] This coupled with the connectivity of the three blocks precludes the formation of the PDMS wetting layer on the top of the microphase-separated thin film, which is well-recognized in PDMS containing block copolymer films.[12,81] As a consequence, the surface morphology could be directly imaged by SEM without the need of short CF_4 plasma etching to remove the PDMS top brush layer (Figure 7A). Moreover, all three components could be distinguished by direct observation with SEM (Figure 7A inset): white (PDMS), gray (PMMA), and PI (dark).

In another example, in contrast to [ALT.LAM] in the bulk, core−shell cylinders appear on silica substrate for DIM-4.9 (Figures 3C and 7B). In this scenario, rather than forming lamellae, as in the bulk, PMMA forms a matrix (Figure 7G), thereby maximizing its interactions with the substrate. The existence of all patterns was confirmed by selective removal of PMMA and PI by isotropic oxygen plasma etching (50 W, 0.3 mbar, 5 min). Upon such treatment PDMS is converted into silicon oxycarbide forming characteristic patterns resistive to

DOI: 10.1021/acs.macromol.7b02485
Macromolecules 2018, 51, 1041−1051

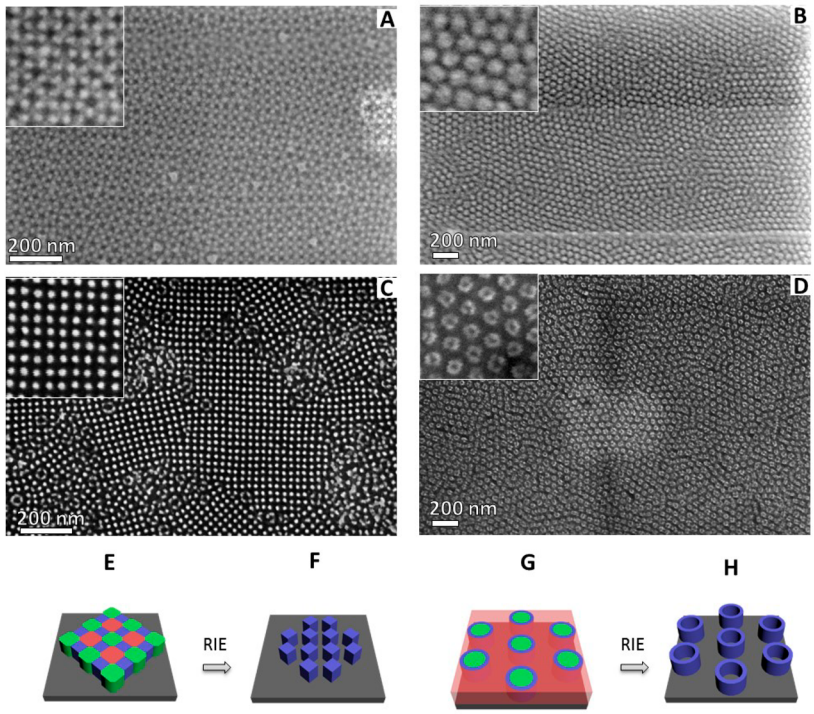

Figure 7. SEM images of the thin films of DIM-2.0 (A, C, E, F) and DIM-4.9 (B, D, G, H) after SVA in acetone (A, B) followed by oxygen plasma etching (C, D, F, H). Bottom row represents computer generated images of the corresponding morphologies before (E, G) and after oxygen plasma etching (F, H). Color code: D = blue, I = green, and M = red.

further oxygen plasma etching (Figure 7C,D,F,H). Both patterns identified in this work, namely, the square array of equally spaced silicon oxycarbide domains (pitch = 25 nm) and the free-standing cylindrical shells of oxidized PDMS (pitch = 53 nm), represent unique surface morphologies unattainable by means of diblock copolymer lithography. Needless to say, the above-mentioned patterns could further be transferred to underlying silica substrate by CF_4 plasma exposure or used as prepared for a range of applications where nanopatterned substrates are required.[82]

As for the samples DIM-0.8 and DIM-13, our attempts to observe their surface patterns were not successful for two possible reasons. In the case of DIM-0.8 the film dewets the substrate immediately after spin coating from toluene solution. Presumably, the low PMMA content in this sample precludes effective adsorption of the DIM-0.8 onto the silicon oxide. For DIM-13, despite the fact that uniform films were always produced via spin coating, reduced chain mobility at such high molecular weight (287 kDa) may account for the inability of the copolymer to form well-defined surface morphologies.

CONCLUSIONS

A series of DIM miktoarm stars consisting of polydimethylsiloxane [D], poly(1,4-isoprene) [I], and poly(methyl methacrylate) [M] arms were synthesized by anionic polymerization using a novel linking agent, 4-allyl-1,1-diphenylethylene. The bulk morphology of DIM was investigated as a function of the volume ratio of M/D = M/I = 0.8−13 while the ratio of D/I was fixed at ∼1. A systematic increase in the molecular weight of the M arm resulted in the morphological transition from [6.6.6] cylindrical tiling to [ALT.LAM] and back to [ALT.CYL] in the bulk. The real space morphologies were determined using TEM, DPD, and SCFT, while SAXS and Fourier transform of SCFT results were used to access the scattering profiles of the polymers. The presence of the PDMS component resistant to oxygen plasma etching allowed us to produce a regular square array of oxidized PDMS dots (pitch = 25 nm) and empty core cylinders (pitch = 53 nm) on silica—the patterns which were drastically different from the observed bulk morphologies. The ability to form regular etch resistant patterns on silica wafers makes synthesized DIM interesting candidates for nanoscopic lithography applications.[12,81,82]

AUTHOR INFORMATION

Corresponding Author

*(S.C.) E-mail: sergeychernyy@gmail.com.

ORCID

Sergey Chernyy: 0000-0002-3214-9454
Jacob Judas Kain Kirkensgaard: 0000-0001-6265-0314
Jyoti P. Mahalik: 0000-0003-4448-4126
Rajeev Kumar: 0000-0001-9494-3488
Bobby G. Sumpter: 0000-0001-6341-0355
Kell Mortensen: 0000-0002-8998-9390
Thomas P. Russell: 0000-0001-6384-5826

Notes

The authors declare no competing financial interest.

ACKNOWLEDGMENTS

S.C., J.J.K.K., and K.A. are thankful to Villum Foundation for the financial support of the project. The help from Lars Schulte is highly appreciated. Support by the Danish National Research Foundation, Project DNRF103, to K.A. and L.S. is acknowledged. Portions of the work-including the computations were conducted at the Center for Nanophase Materials Sciences, which is a US Department of Energy Office of Science User Facility. The Research at Oak Ridge National Laboratory's Spallation Neutron Source was sponsored by the Scientific User

DOI: 10.1021/acs.macromol.7b02485
Macromolecules 2018, 51, 1041−1051

Facilities Division, Office of Basic Energy Sciences, U.S. Department of Energy (DOE). T.P.R. and H.K. were supported by the Air Force Office of Scientific Research under Contract 16RT1602. JPM and MMLA were supported by the Laboratory Directed Research and Development, Technology Innovation Program of ORNL managed by UT-Battelle, LLC for the U.S. Department of Energy.

REFERENCES

(1) Wang, Z.; Li, T.; Schulte, L.; Almdal, K.; Ndoni, S. Photocatalytic Nanostructuring of Graphene Guided by Block Copolymer Self-Assembly. *ACS Appl. Mater. Interfaces* **2016**, *8* (13), 8329−8334.
(2) Phillip, W. A.; O'Neill, B.; Rodwogin, M.; Hillmyer, M. A.; Cussler, E. L. Self-Assembled Block Copolymer Thin Films as Water Filtration Membranes. *ACS Appl. Mater. Interfaces* **2010**, *2* (3), 847−853.
(3) Zhang, Q.; Cirpan, A.; Russell, T. P.; Emrick, T. Donor−Acceptor Poly(thiophene-*block*-perylene diimide) Copolymers: Synthesis and Solar Cell Fabrication. *Macromolecules* **2009**, *42* (4), 1079−1082.
(4) Liddle, J. A.; Gallatin, G. M. Nanomanufacturing: A Perspective. *ACS Nano* **2016**, *10* (3), 2995−3014.
(5) Bates, C. M.; Maher, M. J.; Janes, D. W.; Ellison, C. J.; Willson, C. G. Block Copolymer Lithography. *Macromolecules* **2014**, *47* (1), 2−12.
(6) Bang, J.; Jeong, U.; Ryu, D. Y.; Russell, T. P.; Hawker, C. J. Block Copolymer Nanolithography: Translation of Molecular Level Control to Nanoscale Patterns. *Adv. Mater.* **2009**, *21* (47), 4769−4792.
(7) Barner-Kowollik, C.; Goldmann, A. S.; Schacher, F. H. Polymer Interfaces: Synthetic Strategies Enabling Functionality, Adaptivity, and Spatial Control. *Macromolecules* **2016**, *49* (14), 5001−5016.
(8) Albert, J. N. L.; Epps, T. H., III Self-assembly of block copolymer thin films. *Mater. Today* **2010**, *13* (6), 24−33.
(9) Hamley, I. W. Ordering in thin films of block copolymers: Fundamentals to potential applications. *Prog. Polym. Sci.* **2009**, *34* (11), 1161−1210.
(10) Lane, A. P.; Maher, M. J.; Willson, C. G.; Ellison, C. J. Photopatterning of Block Copolymer Thin Films. *ACS Macro Lett.* **2016**, *5* (4), 460−465.
(11) Li, M.; Ober, C. K. Block copolymer patterns and templates. *Mater. Today* **2006**, *9* (9), 30−39.
(12) Luo, Y.; Montarnal, D.; Kim, S.; Shi, W.; Barteau, K. P.; Pester, C. W.; Hustad, P. D.; Christianson, M. D.; Fredrickson, G. H.; Kramer, E. J.; Hawker, C. J. Poly(dimethylsiloxane-b-methyl methacrylate): A Promising Candidate for Sub-10 nm Patterning. *Macromolecules* **2015**, *48* (11), 3422−3430.
(13) Choi, H. K.; Nunns, A.; Sun, X. Y.; Manners, I.; Ross, C. A. Thin Film Knitting Pattern Morphology from a Miktoarm Star Terpolymer. *Adv. Mater.* **2014**, *26* (16), 2474−2479.
(14) Aissou, K.; Kwon, W.; Mumtaz, M.; Antoine, S.; Maret, M.; Portale, G.; Fleury, G.; Hadziioannou, G. Archimedean Tilings and Hierarchical Lamellar Morphology Formed by Semicrystalline Miktoarm Star Terpolymer Thin Films. *ACS Nano* **2016**, *10* (4), 4055−4061.
(15) Aissou, K.; Choi, H. K.; Nunns, A.; Manners, I.; Ross, C. A. Ordered Nanoscale Archimedean Tilings of a Templated 3-Miktoarm Star Terpolymer. *Nano Lett.* **2013**, *13* (2), 835−839.
(16) Fujimoto, T.; Zhang, H.; Kazama, T.; Isono, Y.; Hasegawa, H.; Hashimoto, T. Preparation and characterization of novel star-shaped copolymers having three different branches. *Polymer* **1992**, *33* (10), 2208−2213.
(17) Okamoto, S.; Hasegawa, H.; Hashimoto, T.; Fujimoto, T.; Zhang, H.; Kazama, T.; Takano, A.; Isono, Y. Morphology of model three-component three-arm star-shaped copolymers. *Polymer* **1997**, *38* (21), 5275−5281.
(18) Bellas, V.; Iatrou, H.; Hadjichristidis, N. Controlled Anionic Polymerization of Hexamethylcyclotrisiloxane. Model Linear and Miktoarm Star Co- and Terpolymers of Dimethylsiloxane with Styrene and Isoprene. *Macromolecules* **2000**, *33* (19), 6993−6997.
(19) Nunns, A.; Ross, C. A.; Manners, I. Synthesis and Bulk Self-Assembly of ABC Star Terpolymers with a Polyferrocenylsilane Metalloblock. *Macromolecules* **2013**, *46* (7), 2628−2635.
(20) Gemma, T.; Hatano, A.; Dotera, T. Monte Carlo Simulations of the Morphology of ABC Star Polymers Using the Diagonal Bond Method. *Macromolecules* **2002**, *35* (8), 3225−3237.
(21) Huang, C.-I.; Fang, H.-K.; Lin, C.-H. Morphological transition behavior of ABC star copolymers by varying the interaction parameters. *Phys. Rev. E* **2008**, *77* (3), 031804.
(22) Kirkensgaard, J. J. K. Striped networks and other hierarchical structures in AmBmCn (2m + n)-miktoarm star terpolymer melts. *Phys. Rev. E* **2012**, *85* (3), 031802.
(23) Xu, W.; Jiang, K.; Zhang, P.; Shi, A.-C. A Strategy to Explore Stable and Metastable Ordered Phases of Block Copolymers. *J. Phys. Chem. B* **2013**, *117* (17), 5296−5305.
(24) Arora, A.; Qin, J.; Morse, D. C.; Delaney, K. T.; Fredrickson, G. H.; Bates, F. S.; Dorfman, K. D. Broadly Accessible Self-Consistent Field Theory for Block Polymer Materials Discovery. *Macromolecules* **2016**, *49* (13), 4675−4690.
(25) Bates, F. S.; Hillmyer, M. A.; Lodge, T. P.; Bates, C. M.; Delaney, K. T.; Fredrickson, G. H. Multiblock Polymers: Panacea or Pandora's Box? *Science* **2012**, *336* (6080), 434−440.
(26) Zhang, G.; Qiu, F.; Zhang, H.; Yang, Y.; Shi, A.-C. SCFT Study of Tiling Patterns in ABC Star Terpolymers. *Macromolecules* **2010**, *43* (6), 2981−2989.
(27) Ueda, K.; Dotera, T.; Gemma, T. Photonic band structure calculations of two-dimensional Archimedean tiling patterns. *Phys. Rev. B: Condens. Matter Mater. Phys.* **2007**, *75* (19), 195122.
(28) Bohbot-Raviv, Y.; Wang, Z.-G. Discovering new ordered phases of block copolymers. *Phys. Rev. Lett.* **2000**, *85* (16), 3428−3431.
(29) Jiang, K.; Zhang, J.; Liang, Q. Self-Assembly of Asymmetrically Interacting ABC Star Triblock Copolymer Melts. *J. Phys. Chem. B* **2015**, *119* (45), 14551−14562.
(30) Li, W.; Xu, Y.; Zhang, G.; Qiu, F.; Yang, Y.; Shi, A.-C. Real-space self-consistent mean-field theory study of ABC star triblock copolymers. *J. Chem. Phys.* **2010**, *133* (6), 064904.
(31) Liu, M.; Li, W.; Qiu, F.; Shi, A.-C. Theoretical study of phase behavior of frustrated ABC linear triblock copolymers. *Macromolecules* **2012**, *45* (23), 9522−9530.
(32) Tyler, C. A.; Morse, D. C. Orthorhombic F d d d Network in Triblock and Diblock Copolymer Melts. *Phys. Rev. Lett.* **2005**, *94* (20), 208302.
(33) Qin, J.; Bates, F. S.; Morse, D. C. Phase behavior of nonfrustrated ABC triblock copolymers: weak and intermediate segregation. *Macromolecules* **2010**, *43* (11), 5128−5136.
(34) Sun, M.; Wang, P.; Qiu, F.; Tang, P.; Zhang, H.; Yang, Y. Morphology and phase diagram of ABC linear triblock copolymers: Parallel real-space self-consistent-field-theory simulation. *Phys. Rev. E* **2008**, *77* (1), 016701.
(35) Tyler, C. A.; Qin, J.; Bates, F. S.; Morse, D. C. SCFT study of nonfrustrated ABC triblock copolymer melts. *Macromolecules* **2007**, *40* (13), 4654−4668.
(36) Erukhimovich, I. Y. Weak segregation theory and non-conventional morphologies in the ternary ABC triblock copolymers. *Eur. Phys. J. E: Soft Matter Biol. Phys.* **2005**, *18* (4), 383−406.
(37) Tang, P.; Qiu, F.; Zhang, H.; Yang, Y. Morphology and phase diagram of complex block copolymers: ABC linear triblock copolymers. *Phys. Rev. E* **2004**, *69* (3), 031803.
(38) Cochran, E. W.; Morse, D. C.; Bates, F. S. Design of ABC triblock copolymers near the ODT with the random phase approximation. *Macromolecules* **2003**, *36* (3), 782−792.
(39) Zheng, W.; Wang, Z.-G. Morphology of ABC triblock copolymers. *Macromolecules* **1995**, *28* (21), 7215−7223.
(40) Nakazawa, H.; Ohta, T. Microphase separation of ABC-type triblock copolymers. *Macromolecules* **1993**, *26* (20), 5503−5511.
(41) Chatterjee, J.; Jain, S.; Bates, F. S. Comprehensive Phase Behavior of Poly(isoprene-b-styrene-b-ethylene oxide) Triblock Copolymers. *Macromolecules* **2007**, *40* (8), 2882−2896.

DOI: 10.1021/acs.macromol.7b02485
Macromolecules 2018, 51, 1041−1051

(42) Kumar, R.; Sides, S. W.; Goswami, M.; Sumpter, B. G.; Hong, K.; Wu, X.; Russell, T. P.; Gido, S. P.; Misichronis, K.; Rangou, S.; Avgeropoulos, A.; Tsoukatos, T.; Hadjichristidis, N.; Beyer, F. L.; Mays, J. W. Morphologies of ABC Triblock Terpolymer Melts Containing Poly(Cyclohexadiene): Effects of Conformational Asymmetry. *Langmuir* **2013**, *29* (6), 1995−2006.
(43) Li, W.; Qiu, F.; Shi, A.-C. Emergence and stability of helical superstructures in ABC triblock copolymers. *Macromolecules* **2012**, *45* (1), 503−509.
(44) Kirkensgaard, J. J. K.; Pedersen, M. C.; Hyde, S. T. Tiling patterns from ABC star molecules: 3-colored foams? *Soft Matter* **2014**, *10* (37), 7182−7194.
(45) Roth, M. Solubility parameter of poly(dimethyl siloxane) as a function of temperature and chain length. *J. Polym. Sci., Part B: Polym. Phys.* **1990**, *28* (13), 2715−2719.
(46) Brandrup, J.; Immergut, E. H.; Grulke, E. A. *Polymer Handbook*, 4th ed.; John Wiley & Sons: New York, 1999; p 2336.
(47) Hayashida, K.; Kawashima, W.; Takano, A.; Shinohara, Y.; Amemiya, Y.; Nozue, Y.; Matsushita, Y. Archimedean Tiling Patterns of ABC Star-Shaped Terpolymers Studied by Microbeam Small-Angle X-ray Scattering. *Macromolecules* **2006**, *39* (14), 4869−4872.
(48) Hayashida, K.; Saito, N.; Arai, S.; Takano, A.; Tanaka, N.; Matsushita, Y. Hierarchical Morphologies Formed by ABC Star-Shaped Terpolymers. *Macromolecules* **2007**, *40* (10), 3695−3699.
(49) Takano, A.; Wada, S.; Sato, S.; Araki, T.; Hirahara, K.; Kazama, T.; Kawahara, S.; Isono, Y.; Ohno, A.; Tanaka, N.; Matsushita, Y. Observation of Cylinder-Based Microphase-Separated Structures from ABC Star-Shaped Terpolymers Investigated by Electron Computerized Tomography. *Macromolecules* **2004**, *37* (26), 9941−9946.
(50) Hayashida, K.; Takano, A.; Arai, S.; Shinohara, Y.; Amemiya, Y.; Matsushita, Y. Systematic Transitions of Tiling Patterns Formed by ABC Star-Shaped Terpolymers. *Macromolecules* **2006**, *39* (26), 9402−9408.
(51) Yamauchi, K.; Takahashi, K.; Hasegawa, H.; Iatrou, H.; Hadjichristidis, N.; Kaneko, T.; Nishikawa, Y.; Jinnai, H.; Matsui, T.; Nishioka, H.; Shimizu, M.; Furukawa, H. Microdomain Morphology in an ABC 3-Miktoarm Star Terpolymer: A Study by Energy-Filtering TEM and 3D Electron Tomography. *Macromolecules* **2003**, *36* (19), 6962−6966.
(52) Tureau, M. S.; Epps, T. H. Effect of Partial Hydrogenation on the Phase Behavior of Poly(isoprene-b-styrene-b-methyl methacrylate) Triblock Copolymers. *Macromolecules* **2012**, *45* (20), 8347−8355.
(53) Ndoni, S.; Papadakis, C. M.; Bates, F. S.; Almdal, K. Laboratory-scale setup for anionic polymerization under inert atmosphere. *Rev. Sci. Instrum.* **1995**, *66* (2), 1090−1095.
(54) Schulz, M. F.; Khandpur, A. K.; Bates, F. S.; Almdal, K.; Mortensen, K.; Hajduk, D. A.; Gruner, S. M. Phase Behavior of Polystyrene−Poly(2-vinylpyridine) Diblock Copolymers. *Macromolecules* **1996**, *29* (8), 2857−2867.
(55) Khandpur, A. K.; Foerster, S.; Bates, F. S.; Hamley, I. W.; Ryan, A. J.; Bras, W.; Almdal, K.; Mortensen, K. Polyisoprene-Polystyrene Diblock Copolymer Phase Diagram near the Order-Disorder Transition. *Macromolecules* **1995**, *28* (26), 8796−8806.
(56) Bates, F. S.; Rosedale, J. H.; Bair, H. E.; Russell, T. P. Synthesis and characterization of a model saturated hydrocarbon diblock copolymer. *Macromolecules* **1989**, *22* (6), 2557−2564.
(57) Varshney, S. K.; Hautekeer, J.; Fayt, R.; Jérôme, R.; Teyssié, P. Anionic polymerization of (meth) acrylic monomers. 4. Effect of lithium salts as ligands on the" living" polymerization of methyl methacrylate using monofunctional initiators. *Macromolecules* **1990**, *23* (10), 2618−2622.
(58) Chernyy, S.; Kirkensgaard, J. J. K.; Bakke, A.; Mortensen, K.; Almdal, K. On the properties of poly(isoprene-b-ferrocenylmethyl methacrylate) block copolymers. *Polymer* **2017**, *133*, 129−136.
(59) Ito, S.; Ishizone, T.; Hirao, A. Precise Synthesis of New Exactly Defined Graft Copolymers Made up of Poly (alkyl methacrylate)s by Iterative Methodology Using Living Anionic Polymerization. *Macromolecules* **2015**, *48* (22), 8307−8314.
(60) Kirkensgaard, J. J. K. Novel network morphologies and compositionally robust 3-colored perforated lamellar phase in A(BC)2 mikto-arm star copolymer melts. *Soft Matter* **2010**, *6* (24), 6102−6108.
(61) Kirkensgaard, J. J. K. Systematic progressions of core-shell polygon containing tiling patterns in melts of 2nd generation dendritic miktoarm star copolymers. *Soft Matter* **2011**, *7* (22), 10756−10762.
(62) Kirkensgaard, J. J. K. Kaleidoscopic tilings, networks and hierarchical structures in blends of 3-miktoarm star terpolymers. *Interface Focus* **2012**, *2* (5), 602−607.
(63) Kirkensgaard, J. J. K.; Evans, M. E.; de Campo, L.; Hyde, S. T. Hierarchical self-assembly of a striped gyroid formed by threaded chiral mesoscale networks. *Proc. Natl. Acad. Sci. U. S. A.* **2014**, *111* (4), 1271−1276.
(64) Grason, G. M.; Kamien, R. D. Self-consistent field theory of multiply branched block copolymer melts. *Phys. Rev. E* **2005**, *71* (5), 051801.
(65) Grason, G. M. The packing of soft materials: Molecular asymmetry, geometric frustration and optimal lattices in block copolymer melts. *Phys. Rep.* **2006**, *433* (1), 1−64.
(66) Tzeremes, G.; Rasmussen, K. Ø.; Lookman, T.; Saxena, A. Efficient computation of the structural phase behavior of block copolymers. *Phys. Rev. E: Stat. Phys., Plasmas, Fluids, Relat. Interdiscip. Top.* **2002**, *65* (4), 041806.
(67) Sides, S. W.; Fredrickson, G. H. Parallel algorithm for numerical self-consistent field theory simulations of block copolymer structure. *Polymer* **2003**, *44* (19), 5859−5866.
(68) https://www.txcorp.com.
(69) Tcherkasskaya, O.; Ni, S.; Winnik, M. A. Direct Energy Transfer Studies of the Domain−Boundary Interface in Polyisoprene−Poly(methyl methacrylate) Block Copolymer Films. *Macromolecules* **1996**, *29* (2), 610−616.
(70) Zartman, G. D.; Wang, S.-Q. A Particle Tracking Velocimetric Study of Interfacial Slip at Polymer−Polymer Interfaces. *Macromolecules* **2011**, *44* (24), 9814−9820.
(71) Mays, J. W.; Kumar, R.; Sides, S. W.; Goswami, M.; Sumpter, B. G.; Hong, K.; Wu, X.; Russell, T. P.; Gido, S. P.; Avgeropoulos, A.; Tsoukatos, T.; Hadjichristidis, N.; Beyer, F. L. Morphologies of poly(cyclohexadiene) diblock copolymers: Effect of conformational asymmetry. *Polymer* **2012**, *53* (22), 5155−5162.
(72) Frigo, M. In *A Fast Fourier Transform Compiler*, Acm sigplan notices, 1999; ACM: 1999; pp 169−180.
(73) Troegel, D.; Stohrer, J. Recent advances and actual challenges in late transition metal catalyzed hydrosilylation of olefins from an industrial point of view. *Coord. Chem. Rev.* **2011**, *255* (13−14), 1440−1459.
(74) Chen, C.; Hecht, M. B.; Kavara, A.; Brennessel, W. W.; Mercado, B. Q.; Weix, D. J.; Holland, P. L. Rapid, Regioconvergent, Solvent-Free Alkene Hydrosilylation with a Cobalt Catalyst. *J. Am. Chem. Soc.* **2015**, *137* (41), 13244−13247.
(75) Itami, K.; Mitsudo, K.; Nishino, A.; Yoshida, J.-i. Metal-Catalyzed Hydrosilylation of Alkenes and Alkynes Using Dimethyl(pyridyl)silane. *J. Org. Chem.* **2002**, *67* (8), 2645−2652.
(76) Matsushita, Y.; Hayashida, K.; Dotera, T.; Takano, A. Kaleidoscopic morphologies from ABC star-shaped terpolymers. *J. Phys.: Condens. Matter* **2011**, *23* (28), 284111.
(77) Ruokolainen, J.; Brinke, G. t.; Ikkala, O. Supramolecular polymeric materials with hierarchical structure-within-structure morphologies. *Adv. Mater.* **1999**, *11* (9), 777−780.
(78) Mortensen, K. Characterization of Polymer Blends and Block Copolymers by Neutron Scattering: Miscibility and Nanoscale Morphology. In *Characterization of Polymer Blends*; Wiley-VCH Verlag GmbH & Co. KGaA: 2014; pp 237−268.
(79) Fasolka, M. J.; Mayes, A. M. Block copolymer thin films: physics and applications. *Annu. Rev. Mater. Res.* **2001**, *31* (1), 323−355.
(80) Matsushita, Y. Creation of Hierarchically Ordered Nanophase Structures in Block Polymers Having Various Competing Interactions. *Macromolecules* **2007**, *40* (4), 771−776.

DOI: 10.1021/acs.macromol.7b02485
Macromolecules 2018, 51, 1041−1051

(81) Jung, Y. S.; Ross, C. A. Orientation-Controlled Self-Assembled Nanolithography Using a Polystyrene−Polydimethylsiloxane Block Copolymer. *Nano Lett.* **2007**, *7* (7), 2046−2050.
(82) Lo, T.-Y.; Dehghan, A.; Georgopanos, P.; Avgeropoulos, A.; Shi, A.-C.; Ho, R.-M. Orienting Block Copolymer Thin Films via Entropy. *Macromolecules* **2016**, *49* (2), 624−633.

DOI: 10.1021/acs.macromol.7b02485
Macromolecules 2018, 51, 1041−1051